

RESEARCH ARTICLE

Pilot Study of the Biological Properties and Vascularization of 3D Printed Bilayer Skin Grafts

Yige Huyan, Qin Lian*, Tingze Zhao, Dichen Li, Jiankang He

State Key Laboratory for Manufacturing System Engineering, School of Mechanical Engineering, Xi'an Jiaotong University, Xi'an, China

Abstract: The skin is the largest human organ, and defects in the skin with a diameter greater than 4 cm do not heal without treatment. Allogeneic skin transplantation has been used to allow wound healing, but many grafts do not survive after implantation, due to multiple complications in the procedure. In the present study, the vascularization of three-dimensional (3D) printed full-thickness skin grafts was investigated. Dermal-epithelial grafts were transplanted into a nude mouse model to evaluate integration with the host tissue and the extent of wound healing. To create microvessels in the skin grafts, a bilayer structure consisting of human dermal fibroblasts, keratinocytes, and microvascular endothelial cells was designed and fabricated using an extruded 3D printer. Human dermal fibroblasts and human microvascular endothelial cells were mixed with gelatin-sodium alginate composite hydrogel as the dermis, and human keratinocytes were mixed with gel as the epithelium. Confocal imaging allowed visualization of the location of the cells in the double-layer skin grafts. A full-thickness wound was created on the backs of nude mice and then covered with a double-layer skin graft. Various groups of mice were tested. Animals were euthanized and tissue samples collected after specified time points. Compared with the control group, wound contraction improved by approximately 10%. Histological analysis demonstrated that the new skin had an appearance similar to that of normal skin and with a significant degree of angiogenesis. The results of the immunohistochemical analysis demonstrated that the transplanted cells survived and participated in the healing process.

Keywords: Three-dimensional printing, Bilayer skin graft, Gelatin-alginate complex hydrogel, Vascularization

*Corresponding Author: Qin Lian, State Key Laboratory for Manufacturing System Engineering, School of Mechanical Engineering, Xi'an Jiaotong University, Xi'an, China; lqiamt@mail.xjtu.edu.cn

Received: November 11, 2019; **Accepted:** January 02, 2020; **Published Online:** January 21, 2020

Citation: Huyan Y, Lian Q, Zhao T, *et al.*, 2020, Pilot study of the biological properties and vascularization of 3D printed bilayer skin grafts. *Int J Bioprint*, 6(1):246. DOI: 10.18063/ijb.v6i1.246

1 Introduction

As the largest human organ, skin^[1] protects the body from poisons, pathogens, microorganisms, and other invaders. It can also regulate homeostasis of body fluids, regulate body temperature, immune monitoring, and self-healing, in addition to, physiological functions such as external sensory stimulation. Human skin consists of epidermis and dermis^[2]. The epidermis is the outermost layer of the skin, of which 90 – 95% of cells are keratinocytes. The dermis lies between the

epidermis and subcutaneous tissue, consisting principally of fibroblasts^[3].

At present, large-area skin defects and chronic skin injury remain major problems in clinics^[4]. Autologous skin transplantation is limited by donor insufficiency, and allografts suffer immune rejection. Tissue-engineered skin is an effective solution^[5]. It can be used not only as a skin substitute in the clinic but also as an infiltration and screening model for basic research. Great progress has been made in the study of tissue-engineered

skin^[6-11]. A variety of commercial tissue-engineered skins have been used clinically^[12]. However, the majority of these products are designed for timely coverage and to promote wound healing, being unable to satisfy every function of the skin. An ideal tissue-engineered skin would exhibit no toxicity or immune rejection, have normal color, include accessory structures, vessels, and nerves, while demonstrating flexibility and appropriate mechanical strength, and able to exchange material and energy^[13-15]. Vascularization of tissue-engineered implants is a key issue that restricts the development of tissue-engineered skin products^[16]. At present, tissue-engineered skin has no vascular structure, its nutritional supply principally relies on osmosis, and hence the thickness is limited. The epidermis is unable to receive sufficient nutrients quickly when the skin thickness is >1 mm, causing partial exfoliation and necrosis of the epidermis.

In the present study, a 3D-printed artificial skin was fabricated which included vascular features and through a series of *in vitro* tests, the cell-hydrogel hybrid material printed by an extrusion printing process was evaluated. The rate of survival of keratinocytes, fibroblasts, and endothelial cells was found to be >90%. In addition, the bilayer skin construct was evaluated *in vivo* by detecting the integration of bilayer skin transplantation with host tissue in a nude mouse model. Nude mice are appropriate in the study of wound healing because they do not suffer immune rejection. In this experiment, a full-thickness wound was created on the back of nude mice. The degree of wound healing contraction rate of mice was close to 90%^[9], significantly different from that of human wounds. However, the nude mouse model exhibited the ability to support the engineered skin transplantation, in addition to allowing measurement of the structural differences between transplanted and normal skin following wound healing. Wound contraction is a part of the normal healing process, but when it is too large, it may lead to dysfunction or esthetic problems in the wounds of patients. The purpose of this study was to compare the *in vivo* response of a number of tissue-engineered skin grafts with different cellular components to non-transplanted skin grafts and to

demonstrate that the tissue-engineered skin graft with vascular endothelial cells is significantly better in wound healing.

2 Materials and methods

2.1 Construction of 3D printed bilayer skin graft

2.1.1 Cell culture and hydrogel preparation

Normal human dermal fibroblasts (NHDFs), human dermal microvascular endothelial cells (HMVECs), and normal human epidermal keratinocytes (NHEKs) were purchased from American type culture collection (ATCC), and maintained and subcultured in accordance with the supplier's protocol. NHDFs were maintained in Dulbecco's Modified Eagle's Medium (DMEM) supplemented with 10% fetal bovine serum (FBS) and 1% antibiotic/antimycotic solution, HMVEC in Roswell Park Memorial Institute (RPMI) 1640 medium supplemented with 10% FBS, and 1% antibiotic/antimycotic solution and NHEKs in Iscove's Modified Dulbecco's Medium (IMDM) supplemented with 10% FBS, and 1% antibiotic/antimycotic solution. Cells were incubated at 37°C in 5% CO₂.

Sodium alginate (Sigma-Aldrich) and gelatin (Sigma-Aldrich) were dissolved in deionized water, heated in a water bath at 37°C, and then stirred with a magnetic stirrer at 80 rpm for 24 h. The gelatin-sodium alginate composite hydrogel solution with 4% (w/v) sodium alginate concentration and 10% (w/v) gelatin concentration was prepared.

2.1.2 Cytotoxicity assay

The hydrogel constructs created in this study were composed of 10% gelatin and 4% sodium alginate. The constructs were placed in DMEM at a 1:10 volume ratio so as to prepare extracts and cultured at 37°C for 24 h^[17]. An improved cell counting kit-8 (CCK-8) cytotoxicity assay (Dojin, Japan) was used to determine cell activity, in accordance with the manufacturer's instructions. NHDFs were plated into the wells of a 96-well plate at a density of 5000 cells per well. Hydrogel extracts were added and incubated with the cells in a humidified atmosphere containing 5% CO₂ at 37°C for 24 h, 48 h, and 72 h. Cells without

hydrogel extract constituted the control. 10 μ l CCK-8 solutions were added to each well of the plate and incubated at 37°C for 4 h. Absorbance at a wavelength of 450 nm was measured using a microplate reader. All results are presented as optical density (OD) values minus the absorbance of blank wells. The distribution of cells was observed using fluorescence microscopy.

2.1.3 3D bioprinter

A custom-built extruded 3D printing equipment consisted of a control system, a mechanism for motion, and feed and nozzle systems (**Figure 1**). The main body of the equipment was placed on an ultra-clean platform. The mechanism providing motion comprised a gantry with four spindles able to move independently in the Z direction. The effective printing range was 100 \times 100 \times 100 mm, with a repeatable precision of 0.05 mm. The feed system was a pneumatic pump.

2.1.4 Live and dead assay

NHDFs were mixed with 10% gelatin and 4% sodium alginate composite hydrogel solution at a

cell density of 1×10^6 cells/ml. The combination of cells and hydrogel was used to print the 3D structure, which was then cultured in a CO₂ incubator at 5% CO₂, 37°C^[18], and evaluated using live and dead staining of the cells on days 1, 4, and 7. Cell growth was observed using a Laser Confocal Microscope (Nikon A1). Live cells appeared green and dead cells red.

2.1.5 Bioprinting of 3D printed bilayer skin graft

NHEKs and a mixture of NHDFs and HMVECs which ratio was 1:1 were separately mixed with 10% gelatin and 4% sodium alginate composite hydrogel solution at each cell density of 1×10^6 cells/ml. A layer of NHEK-hydrogel mixture measuring 20 \times 20 \times 0.5 mm was printed under the printing pressure 0.15 MPA and move speed 15 mm/s in 25°C, representing the epidermal layer of the full-thickness skin, and an additional layer 20 \times 20 \times 0.5 mm was printed using the mixture of NHDFs, HMVECs, and hydrogel as the dermal layer of full-thickness skin (**Figure 2**).

The printed skin grafts were cultured *in vitro* for 1 day before transplantation. The coculture

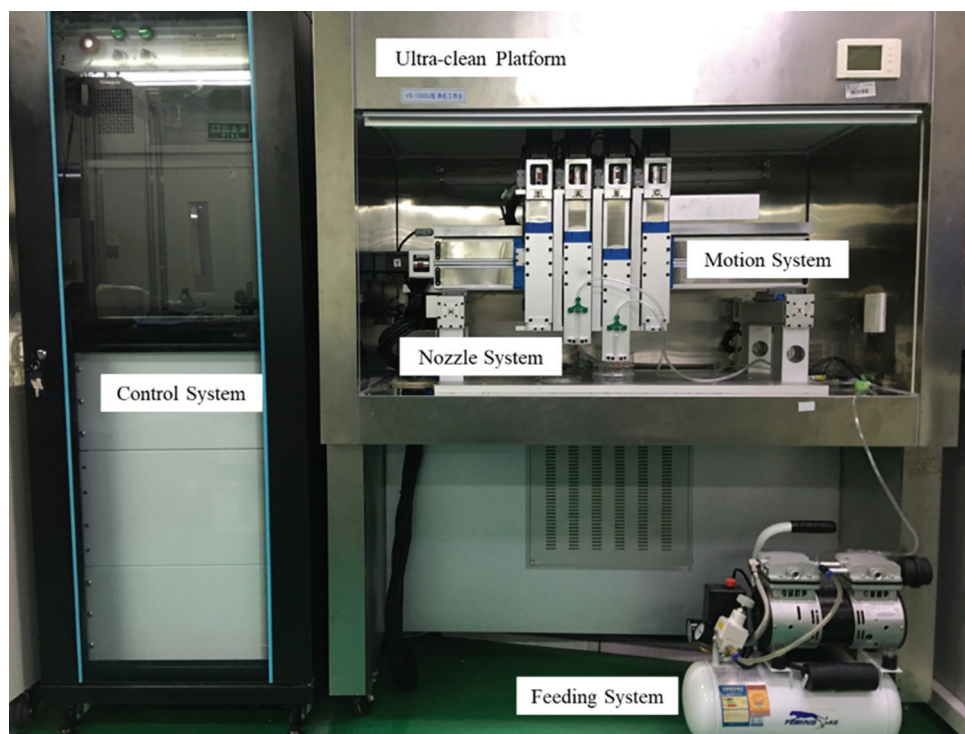


Figure 1. The extruded three-dimensional printing equipment consists of control, motion, feed, and nozzle systems. The main body of the equipment was placed on an ultra-clean platform.

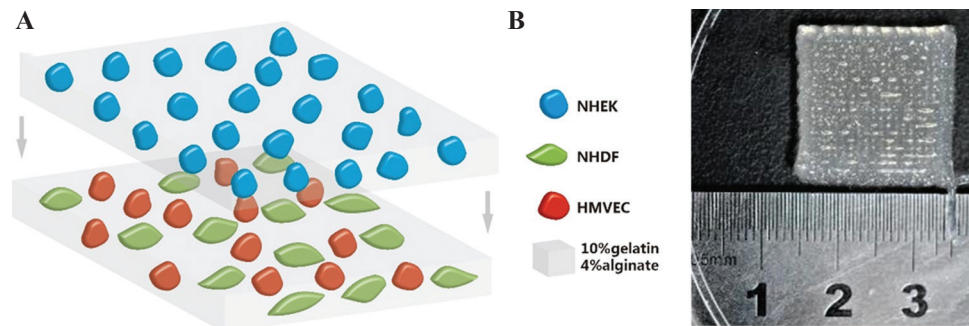


Figure 2. (A) Schematic diagram of transplantable printed skin. The top layer consisted of keratinocytes and gel and the bottom layer fibroblasts, microvascular endothelial cells and gel. (B) A macroscopic image of the printed skin graft.

medium used *in vitro* was the mixed solution of DMEM: IMDM:RPMI = 1:1:1.

2.2 Characterization of the *in vitro* 3D printed bilayer skin graft

NHEKs were labeled with cell Tracker™ Blue 7-amino-4-chloromethylcoumarin dye, in accordance with the manufacturer's protocol. Briefly, the culture medium was removed and pre-warmed cell Tracker Blue (5 μ M of blue dye in 2 ml of serum free media) added and incubated for 15 min at 37°C^[19]. The dye was then removed and the cells incubated with fresh culture medium at 37°C for 30 min. The medium was again removed and the cells washed with phosphate-buffered solution (PBS) labeled cells pass the dye to daughter cells but not adjacent cells. NHDFs were labeled with cell Tracker™ Green 5-chloromethylfluorescein diacetate dye and HMVECs with cell Tracker™ Red CMTPIX dye. The labeling procedure was the same in each case.

2.3 Characterization of the *in vivo* 3D printed bilayer skin graft

2.3.1 Animal surgery

Thirty-two male nude mice were purchased from the SPF Animal Room, Experimental Animal Center of Xi'an Jiaotong University. All experiments had been approved by the Institutional Animal Care and Use Committee of the Ethics Committee of Xi'an Jiaotong University Health Science Center, China. Surgical procedures and post-operative

animal care used sterilized instruments and the procedures were strictly sterile. Mice were anesthetized with ketamine (40–90 mg/kg) and xylazine (5–10 mg/kg) by intraperitoneal injection before surgery. The region for skin grafting was sterilized with iodophor and 75% ethanol. A full-thickness skin incision, 20 \times 20 mm, approximately 1 mm deep, was created on the backs of the nude mice with ophthalmic scissors^[20]. The wounds represented approximately 30–40% of the back of each animal. An aseptic gauze pad was used to halt bleeding of the wound and prevent blood loss exceeding 10–15% of total animal blood volume during surgery. All animals were divided into four groups of eight nude mice each. The printed skin graft was placed within wound so that it completely filled the defect in the experimental group of nude mice. The wound was not grafted in the control group. Tegaderm (3M, London, ON, Canada, <http://www.3m.com>) was placed over the wound to protect the wound site and maintain a moist environment^[21] (**Figure 3**). After surgery, the animals were placed in an aseptic Individual ventilated cage (IVC) containing sterile surgical gauze. The Tegaderm was in place for 8–10 days to ensure that the printed skin had grafted to the tissues of the mice. During this period, infection and the dressings were monitored at least twice per day. The mice were monitored until the experiment had completed, at which time the animals were euthanized and tissue samples collected. Tissues were fixed in 4% paraformaldehyde and then analyzed histologically and with immunohistochemistry.

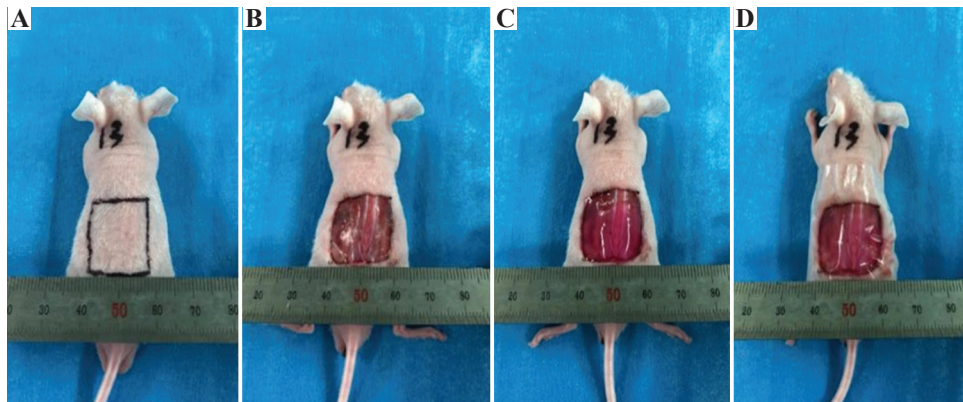


Figure 3. The surgical procedure involved establishing a full-thickness skin wound and transplantation. (A) Marking of the wound incision lines; (B) establishment of a full-thickness skin wound; (C) placement of the printed skin graft; (D) covering by Tegaderm.

2.3.2 Wound contraction

Mice were photographed on the day of surgery and at the end of the experiment. A ruler was placed next to the wound to ensure wounds matched the graft size. The area of the wound at each time point was measured using ImageJ software^[22]. The percentage of wound contraction was defined as follows:

$$\text{wound contraction} = (1 - \text{wound area at end point} / \text{wound area at surgery}) \times 100\%^{[23]}$$

2.3.3 Histology

Tissue samples were harvested at specified times, including the regenerated and contracted skin. The tissue samples were embedded in paraffin wax and cut into 6 μm -thick slices with a microtome then stained with hematoxylin and eosin (H&E)^[24]. The samples were sealed with a glass coverslip and the growth and scar formation of the regenerated skin evaluated by light microscopy, including the formation of microvessels and other skin accessories, and epidermal differentiation. The thickness of the regenerated skin, including the epidermis and dermis, was measured through cross-sectional staining.

2.3.4 Immunohistochemistry

Tissue sections for immunohistochemistry (IHC) were dewaxed in xylene and hydrated in a decreasing gradient of ethanol concentrations (100%, 95%, 70%, 50%, and 0%). Samples were boiled for 15 min in an antigen retrieval solution consisting

of 10 mM sodium citrate, 0.05% polysorbate 20, pH 6.0, cooled for 30 min and washed with $1 \times$ PBS to recover the antigens. The tissue samples were placed in 100 μl normal goat serum and incubated at room temperature for 1 h. An appropriate primary antibody (CD31 YM6277 Immunoway, and CK10 YM6622 Immunoway) diluted in PBS (1: 500) was added to each sample and incubated overnight at 4°C. The samples were washed 5 times with PBS for 5 min each to remove unbound antibody. The samples were incubated with a secondary antibody diluted in PBS (1: 500) for 30 min. The samples were washed in accordance with previously published procedures^[25] then incubated with DAB. The samples were mounted with neutral chewing gum and covered with a coverslip. Finally, staining was observed using a light microscope.

2.4 Statistical analysis

All quantitative data were calculated as arithmetic means and standard deviations. A student's *t*-test was used to compare the skin transplantation samples and control groups at the different time periods. $P < 0.05$ was considered statistically significant.

3 Results

3.1 Cytotoxicity assay

Cytotoxicity evaluation was conducted using a CCK-8 assay to directly determine the effect of the gelatin-alginate composite on the activity of NHDF cells. As shown in **Figure 4**, there

was no significant difference in OD between the experimental and control groups, indicating that the extract had no inhibitory effect on cell growth ($P < 0.05$). Relative growth rate (RGR) was calculated according to the measured OD value. The RGR was between 92.0% and 98.3%, indicating that cytotoxicity was Grade 0 or 1, which is conventionally considered as noncytotoxic.

3.2 Live and dead assay

Confocal microscopy was used to scan cell printed constructs over approximately $1250 \times 1250 \times 300 \mu\text{m}$. The results in **Figure 5** demonstrate that the human dermal fibroblasts grew well and were evenly distributed within the gelatin-alginate composite hydrogel. The cell survival rate was maintained at $>90\%$ by day 7, indicating that the composite hydrogel fulfilled the demands required of a material for printing cells.

3.3 Cell tracking and observation

The results of fluorescent cell tracking are presented in **Figure 6**. Keratinocytes labeled in

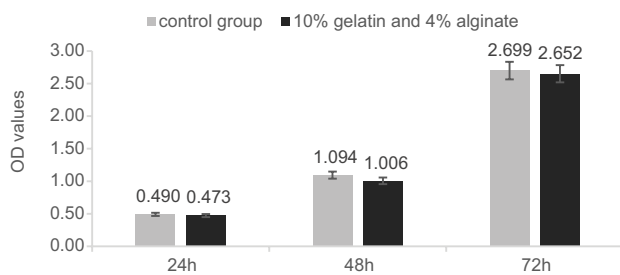


Figure 4. CCK-8 cytotoxicity assay used to assess the cytotoxicity of the hydrogel over 24 h, 48 h, and 72 h on NHDFs.

blue were located on the top layer of the double-layered skin-printed graft, and microvascular endothelial cells and fibroblasts labeled red and green, respectively, were evenly distributed on the bottom layer of a double layer skin graft. *In vitro* culture and observation continued until 7 days after printing. It was observed that the double-layer skin graft maintained normal skin structure, with no apparent microangiogenesis observed, probably due to the lack of the required conditions, such as the inclusion of growth factors in the *in vitro* culture conditions.

3.4 Wound contraction

The wound contraction results are displayed in **Figure 7**. Compared with the size of the wound on the day of surgery, the contraction rate due to the printed skin grafting group (**Figure 7A**) was $79 \pm 6\%$ at 4 weeks. In the blank (**Figure 7D**) and control groups (**Figure 7B and C**), wound contraction was larger than that in the printed skin graft group. After 4 weeks, the wound contraction rate in controls with no endothelial cells was $81 \pm 10\%$, $85 \pm 7\%$ in the acellular controls, and $90 \pm 5\%$ in the blank group. One week after surgery, there was no significant difference in wound contraction between the printed skin grafting group and two control groups which were no endothelial cells and no cells, but the wound area gradually decreased with time. Four weeks after surgery, the wound contraction rate in the printed skin grafting group was significantly lower than that in the blank group and cell-free control group ($P < 0.05$). There was no significant difference in wound contraction between the printed skin

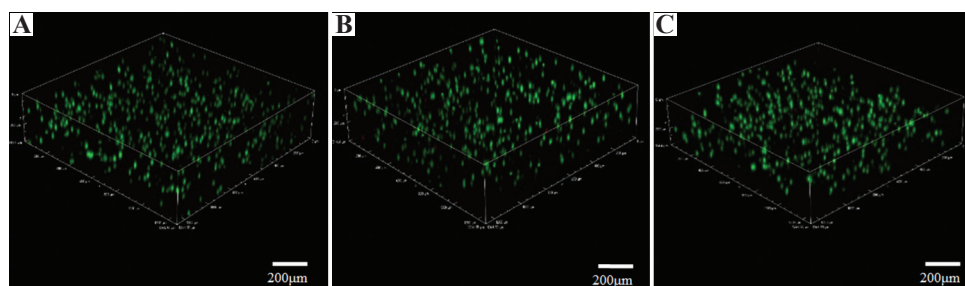


Figure 5. Three-dimensional images of printed cells after live/dead staining. A, B, and C represent cells 1, 4, and 7 days after printing, respectively. Green staining indicates cell survival. Sample dimensions were $1265 \mu\text{m}$ (length) \times $1265 \mu\text{m}$ (width) \times $305 \mu\text{m}$ (height).

transplantation group and the control group without endothelial cells.

3.5 Histology

H&E staining of the different groups 4 weeks after surgery is displayed in **Figure 8**. Histological analysis demonstrated that the printed skin graft group correctly contained all the graft components, with epidermal and dermal structures that were intact. Growth of the printed skin graft group was significantly better than those of the control groups. First, there was significant angiogenesis in the dermis, while there were barely any microvessels in the other groups. Second, the epidermal layer thickness of this group was also significantly greater than the others, a difference that was significant.

3.6 Immunohistochemistry

Immunohistochemical staining of CD31 4 weeks after surgery is shown in **Figure 9**. These results further confirm the histological observations that the printed skin graft group not only exhibited

significant angiogenesis but also that the microvascular-derived cells that were derived from the printed microvascular endothelial cells, confirming that the printed skin graft was capable of growing efficiently and promoting its integration with the mouse tissues and regeneration of blood vessels. **Figure 10** displays immunohistochemical staining of Cytokeratin 10(CK10) 4 weeks after surgery. CK10 identifies the spinous layer of the epidermis and represents one of its major components. Epidermal growth of the printed skin grafting group was significantly greater than those of the control group, with a spinous layer that was significantly thickened.

4 Discussion

The principal purpose of this study was to evaluate the capability of printed skin transplantation to act as a full-thickness skin graft in a full-thickness skin defect model in nude mice. Bioprinting as a highly automated, advanced manufacturing technology^[7], has potential to build tissue-engineered skin with pigment^[26] and sweat glands

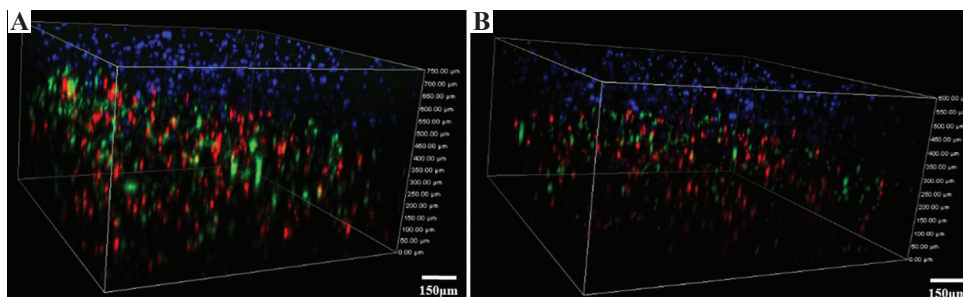


Figure 6. Fluorescent cell tracking in the double skin grafts on the (A) day 1 and (B) day 7 after printing, respectively. Keratinocytes are labeled blue, microvascular endothelial cells red, and fibroblasts green.

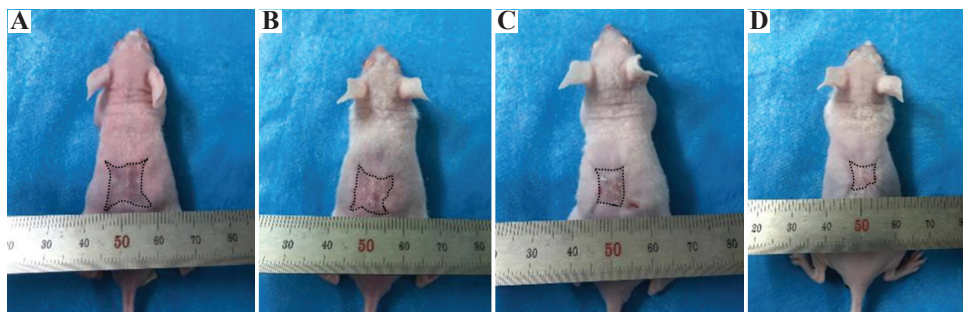


Figure 7. Gross observation of the mice after 4 weeks. A represents the printed skin graft, B is the control group without endothelial cells, C is the control group with no cells, and D is the blank group.

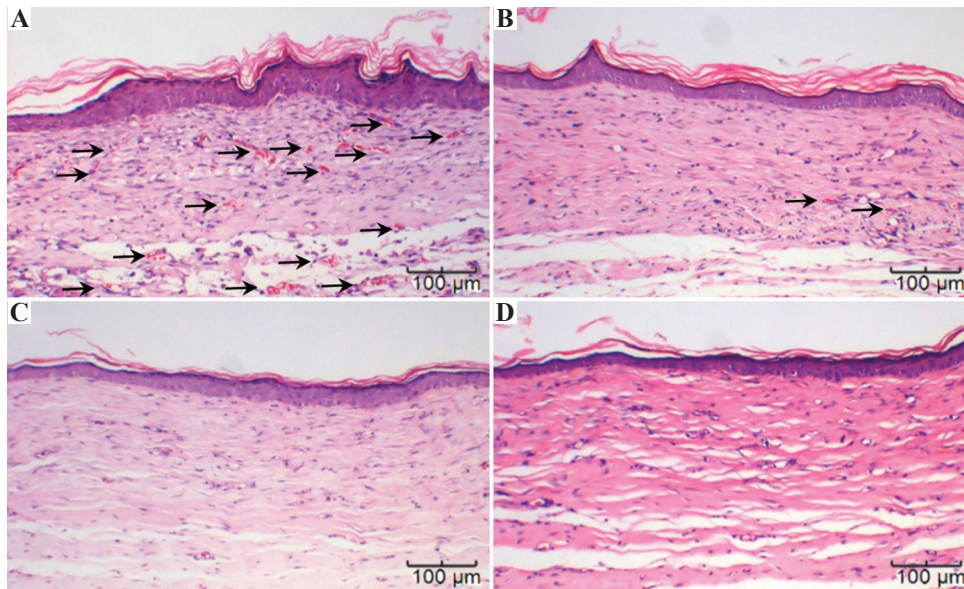


Figure 8: H&E staining of (A) the printed skin graft group with three types of cell; (B) the control group without endothelial cells; (C) the acellular control group; and (D) the blank group.

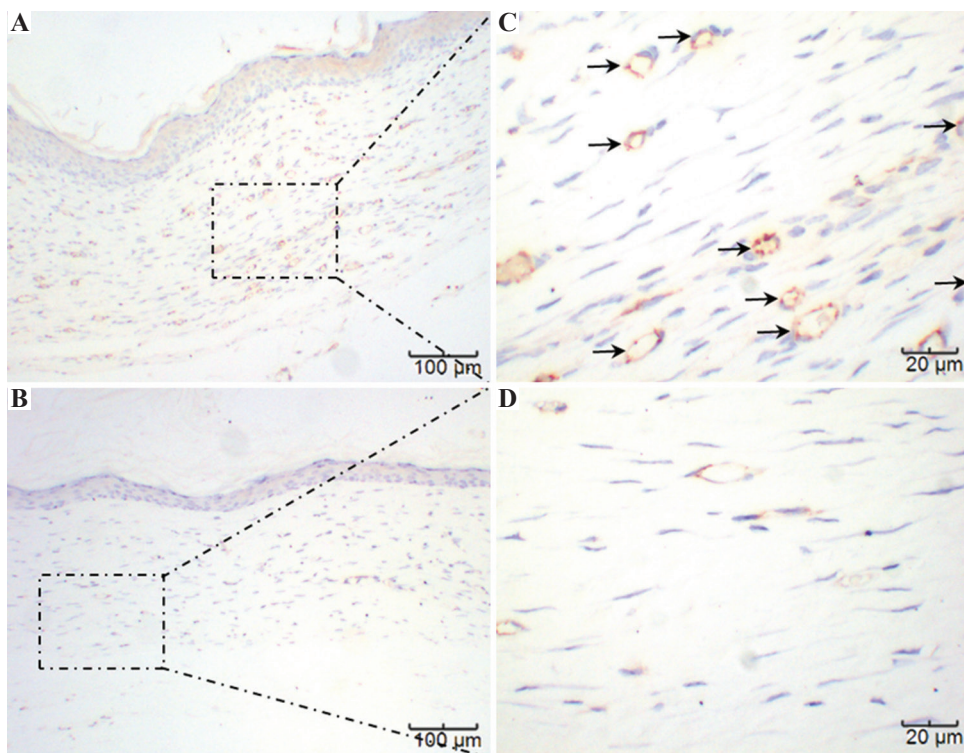


Figure 9. A and C represent the printed skin graft group, at $\times 100$ and $\times 400$, respectively. B and D represent the control group, at $\times 100$ and $\times 400$, respectively. Because there was no significant difference between the three control groups, only one set is displayed. The microvessels marked as brown in A and C can be clearly seen, while visible in B and D only sparsely.

regeneration^[27]. Furthermore, to solve the problems of cell survival and differentiation within the grafts,

prevascularization of the scaffold has become a potential strategy^[28]. Here, we use direct writing

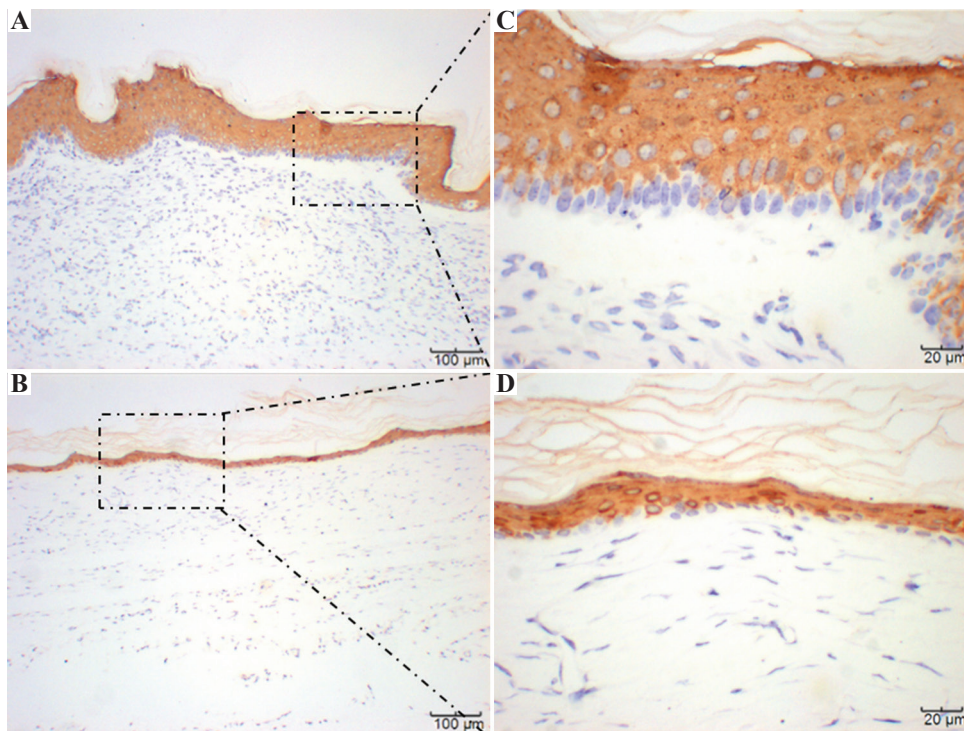


Figure 10. Immunohistochemical staining of CK10. A and C represent the printed skin graft group with HMVECs. B and D represent the control group without HMVECS.

(DW) technology to make a prevascularized skin grafts. First, we developed a composite hydrogel material suitable for printing and transplanting, namely, 10% gelatin and 4% sodium alginate^[29]. Gelatin has excellent biocompatibility but is difficult to print directly at a temperature suitable for cells, while sodium alginate has good performance for printing, but cells can survive within it, they do not function physiologically. We discovered a ratio for the hybrid material that fulfilled both print performance and biocompatibility. The cytotoxicity test results demonstrated good biocompatibility of the composite. In addition, after printing, rather than cross-linking the sodium alginate with calcium ions, an innovative step was to cross-link the gelatin with only the transglutaminase^[29], causing the construct to gradually lose sodium alginate later during culture. In addition, the porosity of the construct increased, allowing greater cell growth and function.

Before performing the animal experiments, we conducted a series of *in vitro* experiments to observe the performance of the printed skin grafts. A live and dead assay demonstrated that the cells

survived well in the material. Fluorescence cell tracking indicated that the double-layer skin graft cultured *in vitro* was able to maintain the printed skin structure over time, with the epidermal and dermal layers clearly demarcated and fibroblasts and microvascular endothelial cells evenly distributed on the bottom layer. However, due to the limitations of the culture conditions, only nutrients derived from the culture medium were present *in vitro*, quite different from normal physiological conditions and so no microvascular formation was observed. As the duration of culture continued, the graft gradually degraded, suggesting that this hybrid hydrogel was an ideal scaffold material^[30].

Wound contraction is a normal part of the healing process^[31], which depends on the age of the animal, wound size, and many other parameters^[32]. Typically, observed wound contraction in human adults is between 20% and 40%, compared with approximately 90% in other mammals such as mice^[33]. Excessive wound contraction leads to joint contracture, local dysfunction, and esthetic problems^[34]. In this study, we found that printing

skin grafts on full-thickness wounds in nude mice improved the degree of wound shrinkage. Wound contraction in the cell groups (printed skin transplantation group and non-endothelial control group) improved to varying degrees compared with the other two groups (cell-free control and blank control groups). However, we did not observe a decrease in wound contraction over time, due to tissue remodeling into normal tissue. The possible reason is that the post-operative observation time was not long enough, but we believe that printing double-layer skin grafts would effectively improve wound contraction in long-term applications.

Histological observations showed that the skin grafts formed epidermal and dermal layers 14 days after surgery, and microvessels are formed, mainly due to the microvascular endothelial cells within the printed skin grafts. In addition, due to the *in vivo* environment providing appropriate stimulation, unlike the *in vitro* environment, such as the presence of relevant growth factors, the printed cells in the skin graft underwent functional phenotypic remodeling. We can be certain that the printed microvascular endothelial cells were involved in the formation of the microvessels during tissue regeneration, but mouse cells may also participate in the repair process through migration or other mechanisms. The majority of other studies have used collagen or other materials as extracellular matrix^[35]. Sodium alginate and gelatin were used in the present study. The good healing response of the animal model and results of histology establish that the use of this hybrid material can achieve excellent results, forming tissue similar to physiological tissue. Microvessel is one of the most important skin appendages^[36]. No other appendages such as hair follicles^[37], sweat glands,^[38] or nerves were observed in this study. We speculate that generation of these appendages may require inclusion of additional components or cells in the printed skin graft. A design that is more rational and closer to the physiological tissue is also required.

5 Conclusions

A gelatin-alginate composite mixed with three skin-specific cell types was manufactured using

direct writing (DW) technology and implanted for the repair of damaged skin on the back of mice in this study. The DW cell-printing process developed by our lab achieved more than a 90% cell survival rate for all three skin-specific cell types and facilitated the manufacture of a bilayer structure which integrated with host tissue within a wound. Animal experimental results indicate that the composite constructs with or without cells can assist skin wound healing, but constructs with cells had the clear advantage of microvessels regeneration. Four weeks after surgery, the constructs containing cells had an approximately 10% increase in wound contraction compared to the other groups, promoting microvessels and skin tissue regeneration, as demonstrated by histological and immunohistochemical analysis.

Acknowledgments

This work was supported by grants from the Science and Technology Projects of PLA (BWS17J036, 18-163-13-ZT-003-011-01) and the National Natural Science Foundation of China (51835010 and 51375371). We thank Health Science Center of Xi'an Jiaotong University for animal experiments, as well as Mr Linian Zhou for his hard work of printing experiments and Mz Lin Gao of histology analysis.

References

1. Rognoni E, Walko G, 2019, The Roles of YAP/TAZ and the Hippo Pathway in Healthy and Diseased Skin. *Cells*, 8(5):E411. DOI: 10.3390/cells8050411.
2. Prost-Squarcioni C, 2006, Histology of Skin and Hair Follicle. *Med Sci (Paris)*, 22(2):131–7. DOI: 10.1051/medsci/2006222131.
3. Bernerd F, 2005, Human Skin Reconstructed *in vitro* as a Model to Study the Keratinocyte, the Fibroblast and Their Interactions: Photodamage and Repair Processes. *J Soc Biol*, 199(4):313–20.
4. Kim SW, Choi SH, Kim JT, *et al.*, 2015, An Additional Option for Split-Thickness Skin Graft Donors: The Previous Free Flap Sites. *Ann Plast Surg*, 75(6):634–6. DOI: 10.1097/SAP.000000000000143.
5. Wei LG, Chang HI, Wang Y, *et al.*, 2019, A Gelatin/Collagen/ Polycaprolactone Scaffold for Skin Regeneration. *PeerJ*,

- 7:e6358. DOI: 10.7717/peerj.6358.
6. Han XX, Courseaus J, Khamassi J, et al., 2018, Optimized Vascular Network by Stereolithography for Tissue Engineered Skin. *Int J Bioprinting*, 4(2):17. DOI: 10.18063/IJB.v4i2.134.
 7. Ng WL, Chua CK, Shen YF, 2019, Print Me An Organ! Why We Are Not There Yet. *Prog. Polym Sci*, 97:45. DOI: 10.1016/j.progpolymsci.2019.101145.
 8. Liu F, Liu C, Chen QH, et al., 2018, Progress in Organ 3D Bioprinting. *Int J Bioprinting*, 4(1):15. DOI: 10.18063/IJB.v4i1.128.
 9. An J, Teoh JEM, Suntornmond R, et al., 2015, Design and 3D Printing of Scaffolds and Tissues. *Engineering*, 1(2):261–8. DOI: 10.15302/j-eng-2015061.
 10. Choudhury D, Anand S, Naing MW, 2018, The Arrival of Commercial Bioprinters Towards 3D Bioprinting Revolution! *Int J Bioprinting*, 4(2):20. DOI: 10.18063/IJB.v4i2.139.
 11. Zhuang P, Sun AX, An J, et al., 2018, 3D Neural Tissue Models: From Spheroids to Bioprinting. *Biomaterials*, 154:113–33. DOI: 10.1016/j.biomaterials.2017.10.002.
 12. Chong C, Wang Y, Fathi A, et al., 2019, Skin Wound Repair: Results of a Pre-clinical Study to Evaluate Electropun Collagen-Elastin-PCL Scaffolds as Dermal Substitutes. *Burns*, 45(7):1639–48. DOI: 10.1016/j.burns.2019.04.014.
 13. Kandhasamy S, Arthi N, Arun RP, et al., 2019, Synthesis and Fabrication of Novel Quinone-Based Chromenopyrazole Antioxidant-Laden Silk Fibroin Nanofibers Scaffold for Tissue Engineering Applications. *Mater Sci Eng C Mater Biol Appl*, 102:773–87. DOI: 10.1016/j.msec.2019.04.076.
 14. Baltazar T, Merola J, Catarino C, et al., 2019, Three Dimensional Bioprinting of a Vascularized and Perfusable Skin Graft Using Human Keratinocytes, Fibroblasts, Pericytes, and Endothelial Cells. *Tissue Eng Part A*, 12. DOI: 10.1089/ten.tea.2019.0201.
 15. Ng WL, Yeong WY, 2019, The Future of Skin Toxicology Testing Three-Dimensional Bioprinting Meets Microfluidics. *Int J Bioprinting*, 5(2.1):44–54. DOI: 10.18063/ijb.v5i2.1.237.
 16. Wang JH, Chen J, Kuo SM, et al., 2019, Methods for Assessing Scaffold Vascularization *In Vivo*. *Methods Mol Biol*, 1993:217–26. DOI: 10.1007/978-1-4939-9473-1_17.
 17. Li Y, Lu H, Gu Y, et al., 2017, Enhancement of NK Cells Proliferation and Function by Shikonin. *Immunopharmacol Immunotoxicol*, 39(3):124–30. DOI: 10.1080/08923973.2017.1299174.
 18. Zhou S, Cui Z, Urban J, 2011, Dead Cell Counts During Serum Cultivation are Underestimated by the Fluorescent Live/Dead Assay. *Biotechnol J*, 6(5):513–8. DOI: 10.1002/biot.201000254.
 19. Kuppam P, Sethuraman S, Krishnan UM, 2017, *In Vitro* Co-Culture of Epithelial Cells and Smooth Muscle Cells on Aligned Nanofibrous Scaffolds. *Mater Sci Eng C Mater Biol Appl*, 81:191–205. DOI: 10.1016/j.msec.2017.07.050.
 20. Yanez M, Rincon J, Dones A, et al., 2015, *In Vivo* Assessment of Printed Microvasculature in a Bilayer Skin Graft to Treat Full-Thickness Wounds. *Tissue Eng Part A*, 21(1-2):224–33. DOI: 10.1089/ten.TEA.2013.0561.
 21. Nye R, Robinia K, Peterson P, et al., 2018, Efficacy of a Nitric Oxide Dressing in Decreasing Bacterial Counts on Human Skin. *J Wound Care*, 27(7):S19–25. DOI: 10.12968/jowc.2018.27.Sup7.S19.
 22. Garcia M, Escamez MJ, Carretero M, et al., 2007, Modeling Normal and Pathological Processes Through Skin Tissue Engineering. *Mol Carcinog*, 46(8):741–5. DOI: 10.1002/mc.20327.
 23. Yannas IV, Tzeranis DS, So PTC, 2017, Regeneration of Injured Skin and Peripheral Nerves Requires Control of Wound Contraction, not Scar Formation. *Wound Repair Regen*, 25(2):177–91. DOI: 10.1111/wrr.12516.
 24. Feldman AT, Wolfe D, 2014, Tissue Processing and Hematoxylin and Eosin Staining. *Methods Mol Biol*, 1180:31–43. DOI: 10.1007/978-1-4939-1050-2_3.
 25. Ferringer T, 2015, Immunohistochemistry in Dermatopathology. *Arch Pathol Lab Med*, 139(1):83–105. DOI: 10.5858/arpa.2014-0075-RA.
 26. Ng WL, Qi JTZ, Yeong WY, et al., 2018, Proof-of-Concept: 3D Bioprinting of Pigmented Human Skin Constructs. *Biofabrication*, 10(2):025005. DOI: 10.1088/1758-5090/aa9e1e.
 27. Huang S, Yao B, Xie J, et al., 2016, 3D Bioprinted Extracellular Matrix Mimics Facilitate Directed Differentiation of Epithelial Progenitors for Sweat Gland Regeneration. *Acta Biomater*, 32: 170–7. DOI: 10.1016/j.actbio.2015.12.039.
 28. Kim BS, Kwon YW, Kong JS, et al., 2018, 3D Cell Printing of *In Vitro* Stabilized Skin Model and *In Vivo* Pre-Vascularized Skin Patch Using Tissue-Specific Extracellular Matrix Bioink: A Step Towards Advanced Skin Tissue Engineering. *Biomaterials*, 168:38–53. DOI: 10.1016/j.biomaterials.2018.03.040.
 29. Chen H, Xing X, Tan H, et al., 2017, Covalently Antibacterial Alginate-Chitosan Hydrogel Dressing Integrated Gelatin Microspheres Containing Tetracycline Hydrochloride for Wound Healing. *Mater Sci Eng C Mater Biol Appl*, 70:287–95. DOI: 10.1016/j.msec.2016.08.086.
 30. Nezhad ZM, Poncelet A, Fervaille C, et al., 2019, Comparing

- the Host Reaction to CorMatrix and Different Cardiac Patch Materials Implanted Subcutaneously in Growing Pigs. *Thorac Cardiovasc Surg*, 67(1):44–9. DOI: 10.1055/s-0037-1607332.
31. Limandjaja GC, van den Broek LJ, Breetveld M, *et al.*, 2018, Characterization of *In Vitro* Reconstructed Human Normotrophic, Hypertrophic, and Keloid Scar Models. *Tissue Eng Part C Methods*, 24(4):242–53. DOI: 10.1089/ten.TEC.2017.0464.
 32. Walmsley GG, Hu MS, Hong WX, *et al.*, 2015, A Mouse Fetal Skin Model of Scarless Wound Repair. *J Vis Exp*, 95:52297. DOI: 10.3791/52297.
 33. Tranquillo RT, Murray JD, 1993, Mechanistic Model of Wound Contraction. *J Surg Res*, 55(2):233–47. DOI: 10.1006/jsre.1993.1135.
 34. Oosterwijk AM, Mouton LJ, Schouten H, *et al.*, 2017, Prevalence of Scar Contractures After Burn: A Systematic Review. *Burns*, 43(1):41–9. DOI: 10.1016/j.burns.2016.08.002.
 35. Lee V, Singh G, Trasatti J P, *et al.*, 2014, Design and Fabrication of Human Skin by Three-Dimensional Bioprinting. *Tissue Eng Part C Methods*, 20(6):473–84. Doi: 10.1089/ten.TEC.2013.0335.
 36. Lee MS, Ahmad T, Lee J, *et al.*, 2017, Dual Delivery of Growth Factors with Coacervate-Coated Poly(Lactic-Co-Glycolic Acid) Nanofiber Improves Neovascularization in a Mouse Skin Flap Model. *Biomaterials*, 124:65–77. Doi: 10.1016/j.biomaterials.2017.01.036.
 37. Lalley AL, Boyce ST, 2019, Fabrication of Chimeric Hair Follicles for Skin Tissue Engineering. *Methods Mol Biol*, 1993:159–79. DOI: 10.1007/978-1-4939-9473-1_13.
 38. Brandenburger M, Kruse C, 2019, Fabrication of a Co-Culture System with Human Sweat Gland-Derived Cells and Peripheral Nerve Cells. *Methods Mol Biol*, 1993:139–48. DOI: 10.1007/978-1-4939-9473-1_11.